DOI: 10.1002/cctc.201500161

Hydrothermal Preparation of a Robust Boehmite-Supported *N*,*N*-Dimethyldodecylamine *N*-Oxide-Capped Cobalt and Palladium Catalyst for the Facile Utilization of Formic Acid as a Hydrogen Source

Hemant Choudhary, Shun Nishimura, and Kohki Ebitani*[a]

Bimetallic CoPd nanoparticles (NPs) on boehmite (AlOOH) were synthesized under hydrothermal conditions using three different capping agents for the facile utilization of formic acid (FA) as a hydrogen source. The CoPd NPs capped with *N*,*N*-dimethyldodecylamine *N*-oxide (DDAO) supported on AlOOH (CoPd-DDAO/AlOOH) exhibited superior catalysis and recyclability in the hydrogenation of maleic anhydride (MAn) in water without metal leaching. The formation of monodispersed CoPd-DDAO NPs on AlOOH that contained both cobalt oxides and CoPd alloy in each NP was indicated by TEM with energy-dispersive spectroscopy, XRD, and X-ray absorption spectroscopy (XAS) studies. X-ray photoelectron spectroscopy and XAS supported the partial electron transfer phenomenon in CoPd-DDAO NPs. The as-prepared CoPd-DDAO/AlOOH catalyst showed activity for the utilization of FA formed in situ from biomass for the hydrogenation of MAn. It suggested that the DDAO capping agent contributed strongly to the favorable electronic/geometric changes in CoPd alloy for the facile utilization of FA.

Introduction

Recent research to overcome economic hurdles in fuel cell technology has introduced various systems for the catalytic dehydrogenation of formic acid (FA) into hydrogen.[1–6] FA is a sustainable and convenient hydrogen storage material[7–11] that can be obtained from biomass in high yields.[12–15] In spite of the spectacular research accomplishments in the dehydrogenation of FA, limited efforts have been made to replace hazardous H_2 by FA in catalytic hydrogenation reactions. However, the scope for the synthesis of efficacious heterogeneous catalysts is wide, and supported metal nanoparticles (NPs) are of prime interest. The resulting interactions of dispersed NPs on a support and their impact on the composition, structure, and catalytic performances of NPs have been well understood in the past decades.[16–20] It has been reported that not only the metal–support interactions but also the type of capping agent influences the electronic properties of NPs.[16–20] Pd-based catalysts are more efficient for FA decomposition than the overpriced Pt catalysts used commonly because of the facilitated two-electron oxidation step of FA that promotes the dehydrogenation pathway (toward H_2 and CO_2) rather than the dehydration pathway (toward H_2O and CO).[21,22] Unfortunately, the limiting step is the adsorption/dissociation of FA on the Pd catalyst surface, which demands increased quantities of catalyst (and in turn increases cost) to achieve a high catalytic activity. Of late, it has been found that the incorporation of an earlier transition metal can enhance the two-electron oxidation process dramatically because of their oxophilic properties.[6] Similar effects of alloying Pd with transition metals have been observed for the oxygen reduction reaction.[23–25]

A significant accomplishment has been made in the synthesis of colloidal NPs using various methods,[26–35] and some studies exist for the simple synthesis of stable supported MPd (M = Fe, Ni, Co, Au, Ru) alloy NPs for catalytic research.[17,18,36–38] Homogeneous polymer-protected metal NPs have the advantages of a high degree of dispersion with serious issues of separation and sustainability for wider applications. Thus, it becomes necessary to develop stable and highly active heterogeneous NP (or supported NP) catalysts.

Hydrothermal methods have gained popularity in the synthesis of advanced materials, which include nanomaterials, mainly because of the reasonable product quality (narrow size distribution and good crystallinity) and high reproducibility.[39–41] Recently, we synthesized a CuO_x NPs supported on MgO catalyst using cetyltrimethylammonium bromide (CTAB) as a capping agent (denoted as Cu-CTAB/MgO) by a simple hydrothermal methodology to obtain a stable and active catalyst for the synthesis of FA and lactic acid from biomass resources.[15] These results motivated us to extend the preparation method for a bimetallic catalyst such as CoPd and to examine its catalytic activity for the industrially important maleic anhydride (MAn) hydrogenation reaction toward succinic acid (SA), a C-4 building block chemical.[42] Very recently, our group synthesized supported metal catalysts for efficient utilization of FA

---

[a] *H. Choudhary, Dr. S. Nishimura, Prof. Dr. K. Ebitani
School of Materials Science
Japan Advanced Institute of Science and Technology
1-1 Asahidai, Nomi, Ishkawa 923 1292 (Japan)
E-mail: ebitani@jaist.ac.jp*

Supporting Information for this article is available on the WWW under http://dx.doi.org/10.1002/cctc.201500161.

in the hydrogenation reactions of 5-hydroxymethylfuraldehyde, levulinic acid, and nitroarenes.[43–45] Continuous research efforts in the effective and facile utilization of FA under moderate conditions with decreased metal content for industrially important catalytic reactions paved the path for this research.

As pioneers in this field, Toshima et al. have reported the role of poly(*N*-vinyl-2-pyrrolidone) (PVP) on the geometric, physical, and chemical properties of NPs.[46–49] Our group has also demonstrated PVP,[18] acrylate,[50] starch,[19–20] and CTAB[15] as efficient capping agents that influence the formation mechanism of NPs and/or the properties of the constructed active centers on supported NP catalysts.

For the hydrothermal synthesis of the CoPd catalyst in this study, we chose *N*,*N*-dimethyldodecylamine *N*-oxide (DDAO; Figure 1), a nonionic surfactant, as the capping agent. As DDAO possesses strong hydrophilicity and a similar functionality to PVP, it is expected to affect both the physical and chemical properties of the produced NPs.

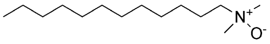

Figure 1. Chemical structure of DDAO.

Herein, we demonstrate the preparation (under hydrothermal conditions) and superior catalysis of a robust supported, capped, bimetallic CoPd catalyst for the hydrogenation of MAn to SA using FA as an inexpensive and sustainable hydrogen source. The characterization of the DDAO-stabilized bimetallic CoPd NPs by TEM, XRD, X-ray photoelectron spectroscopy (XPS), and X-ray absorption spectroscopy (XAS) and the one-pot synthesis of SA using FA formed from glucose are also described.

Results and Discussion

Hydrogenation of MAn to SA using FA

The hydrogenation of MAn, an industrially important pathway to produce SA,[42] was chosen as the test reaction to evaluate the catalytic activity of supported mono- and bimetallic catalysts. The hydrogenation was performed using FA as a hydrogen source. DDAO-capped bimetallic CoPd NPs supported on AlOOH (CoPd-DDAO/AlOOH) exhibited excellent catalytic activity for the selective hydrogenation of MAn to SA (>99% yield; Table 1, entry 1).[51] The superiority of the bimetallic CoPd catalyst was established by experiments performed with the corresponding monometallic Pd or Co catalysts prepared by same procedure (entries 2–3). Pd-DDAO/AlOOH possessed some catalytic activity (29% yield) for the hydrogenation reaction, whereas Co-DDAO/AlOOH failed to show any activity even after 5 h of reaction time.

To elucidate the effect of the DDAO capping agent, CoPd catalysts with and without other common capping agents were also prepared by the same procedure. From our previous studies on the use of capping agents, we selected CTAB[15] and PVP[18] to compare with DDAO. However, the CoPd catalysts capped with CTAB or PVP hardly facilitated the hydrogenation reaction with FA (≈35% yields; Table 1, entries 5–6). Fumaric acid was observed as the only byproduct in some of the catalytic hydrogenations of MAn under our reaction conditions.

The real Co loadings were in the range of 0.55–1.02 wt%, which were much lower than the theoretical value (2.5 wt%) in all of the Co catalysts (entries 1 and 3–6). The molar compositions of the capped CoPd catalyst from inductively coupled plasma atomic emission spectroscopy (ICP-AES) were found to be $Co_{0.23}Pd_{0.77}$-DDAO/AlOOH (i.e., 0.75 wt% Co and 2.53 wt% Pd loading), $Co_{0.20}Pd_{0.80}$-CTAB/AlOOH, and $Co_{0.18}Pd_{0.82}$-PVP/AlOOH. The loading amount of Co cannot explain the differences between the catalysts.

The noncapped CoPd catalyst, $Co_{0.28}Pd_{0.72}$/AlOOH estimated by ICP-AES, had considerable activity (56% yield) in the first run with a high Co loading (entry 4). However, significant Co leaching was observed after the first catalytic cycle; the initial loaded amount of Co (0.94 wt%) decreased drastically to 0.39 wt% (entry 4e). Thus, Co species were hardly preserved on catalyst surface during the reaction without a capping agent. In other words, this result established the efficiency of DDAO to retain metal species on AlOOH during the catalytic runs.

Table 1. Hydrogenation of MAn using FA.[a]

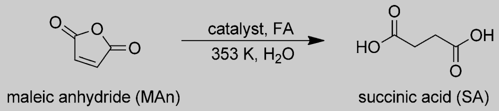

Entry	Catalyst	Time [h]	Co [wt%][b]	Pd [wt%][b]	Conversion [%][c]	Yield [%][c]
1	CoPd-DDAO/AlOOH	3	0.75, 0.71[d]	2.53, 2.52[d]	>99, >99[d]	>99, >99[d]
2	Pd-DDAO/AlOOH	5	0	2.64	40	29
3	Co-DDAO/AlOOH	5	1.02	0	0	0
4	CoPd/AlOOH	3	0.94, 0.39[e]	2.44, 2.41[e]	72	56
5	CoPd-CTAB/AlOOH	3	0.63	2.49	52	36
6	CoPd-PVP/AlOOH	3	0.55	2.51	4	35
7	Pd/Al_2O_3 (commercial)	3	0	5[f]	98	74
8[g]	CoPd-DDAO/AlOOH	3	0.75	2.53	>99	>99
9	AlOOH	3	0	0	0	0
10	blank	3	0	0	0	0
11[h]	CoPd-DDAO/AlOOH	3	0.75	2.53	0	0
12[i]	CoPd-DDAO/AlOOH	3	0.75	2.53	>99	98

[a] Reaction conditions: MAn (0.5 mmol), FA (1.9 mmol), catalyst (25 mg), 353 K, H_2O (5 mL), Teflon-lined autoclave. [b] Determined by ICP-AES. [c] Calculated by HPLC using a calibration curve method. [d] Fifth catalytic run. [e] After the first catalytic run. [f] Quoted from the manufacturer's product specifications. [g] H_2 (0.1 MPa). [h] Without FA. [i] 2,6-Di-*tert*-butyl-*p*-cresol (0.15 mmol) was used as a radical scavenger.

The 5 wt% Pd/Al_2O_3 commercial catalyst afforded a high conversion (98%) because of the high Pd amount with moderate SA yields (74%; entry 7). CoPd-DDAO/AlOOH also hydrogenated MAn efficiently in the presence of H_2 (entry 8). The reaction could not progress in the absence of Pd at all (entries 3, 9, and 10), which indicates that the Pd species acted as the active center for the catalysis. Without FA (hydrogen source), the reaction did not proceed (entry 11). The catalytic activity was investigated carefully as a function of temperature, time, and the amount of FA in the reaction medium (Tables S1 and S2 and Figure S1). Then, 3 h and 353 K with 1.9 mmol of FA were found to be the best reaction conditions for MAn hydrogenation over CoPd-DDAO/AlOOH. Notably, CoPd-DDAO/AlOOH retained a high catalytic activity even after the fifth run of hydrogenation (Table 1, entry 1d and Figure S2). It was ascertained that CoPd-DDAO/AlOOH had a similar composition to $Co_{0.22}Pd_{0.78}$-DDAO/AlOOH (i.e., 0.71 wt% Co and 2.52 wt% Pd loading) even after five runs (entry 1 d).[52]

To understand the nature of FA dissociation and clarify the reaction pathway over CoPd-DDAO/AlOOH, a radical scavenger was added to the reaction mixture. The result in Table 1, entry 12 showed that there was no influence of the radical scavenger (2,6-di-*tert*-butyl-*p*-cresol, 0.15 mmol) on the hydrogenation of MAn using FA over the CoPd-DDAO/AlOOH catalyst. These results ruled out the possibility of any radical intermediate (hydrogen radical or carbon-centered free radical) within the reaction medium. Additionally, the gaseous products after the treatment of only FA (without MAn) with CoPd-DDAO/AlOOH were collected and analyzed by GC with thermal conductivity detection (TCD) and an active carbon column. Although a peak that corresponds to CO_2 was detected, no signals for H_2 appeared in the chromatogram (Figure S3). The dissociation of FA to CO_2 by a dehydrogenation pathway[22] and the presence of adsorbed hydrogen as an ionic species in our reaction medium are proposed from these observations.

TEM of CoPd-capped/AlOOH

TEM was measured to characterize the bimetallic CoPd NPs. Typical TEM images and particle size distributions of capped and noncapped bimetallic CoPd NPs on AlOOH and the commercial Pd/Al_2O_3 catalyst are shown in Figure 2. Well-dispersed and well-shaped NPs were obtained for all catalysts. Interestingly, the DDAO-capped bimetallic CoPd NPs exhibited a wider particle size distribution with an average diameter of 6.4 nm (Figure 2a and g) than the other bimetallic CoPd NPs. CTAB-capped CoPd NPs afforded the biggest size of 7.5 nm (Figure 2b and h), whereas noncapped CoPd NPs had an average diameter of 5.5 nm (Figure 2d and j). PVP-capped CoPd NPs exhibited an intermediate average particle size of 6.2 nm (Figure 2c and i). These results suggest that the formation process and/or the growth rate of bimetallic CoPd NPs varies in the presence of capping agents under the hydrothermal conditions. TEM images for commercial 5 wt% Pd/Al_2O_3 showed

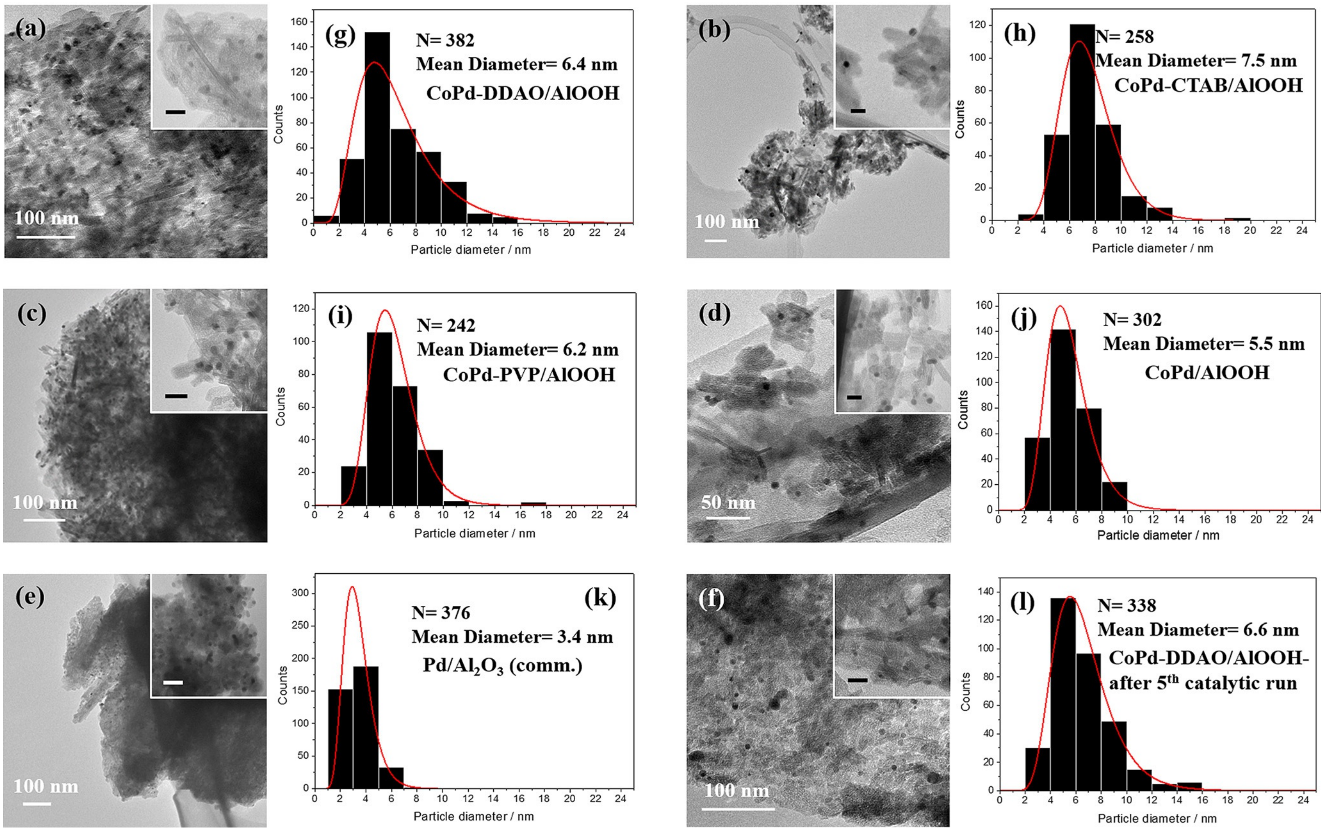

Figure 2. a–f) TEM images and g–l) particle size distributions of a, g) CoPd-DDAO/AlOOH, b, h) CoPd-CTAB/AlOOH, c, i) CoPd-PVP/AlOOH, d, j) CoPd/AlOOH, e, k) Pd/Al_2O_3, and f, l) CoPd-DDAO/AlOOH after the fifth catalytic run. Inset shows the TEM images at higher magnifications (scale bar is 20 nm).

a narrow particle size distribution and a mean particle diameter of 3.4 nm (Figure 2e and k). The TEM images and size distribution of CoPd-DDAO/AlOOH after the fifth catalytic run were similar to those of the fresh catalyst (cf. Figure 2a and g and 2f and l), which demonstrates the stability of the catalyst capped with DDAO. TEM images of the DDAO-capped monometallic catalyst and the bare support (AlOOH) were also recorded (Figure S4).

The high-angle annular dark-field scanning transmission electron microscopy (HAADF-STEM) images shown in Figure S5 reveal the crystalline nature of CoPd-DDAO/AlOOH. The compositional mapping was performed by STEM with energy-dispersive spectroscopy (EDS) mapping and HAADF-STEM. Inspection of the elemental mapping image shows the uniform distribution of Co and Pd elements within the bimetallic CoPd NPs with a higher concentration of Pd than Co. The HAADF-STEM line analysis shown in Figure S5 suggests the composition is $Co_{0.1}Pd_{0.9}$. Similar results in elemental mapping images were observed at various places, which demonstrate the homogeneity of the bimetallic CoPd NPs (consistent compositional distribution within each NP) throughout the catalyst structure. The existence of bimetallic CoPd NPs over the AlOOH surface as an alloy is substantiated by STEM. At some places darker and brighter regions were observed on the NPs, however, the line analysis disproved the formation of a core–shell structure. However, the composition of the NPs estimated by STEM-EDS line analysis ($Co_{0.1}Pd_{0.9}$) differed from that from ICP-AES ($Co_{0.23}Pd_{0.77}$). This implied that the $Co_{0.23}Pd_{0.77}$-DDAO/AlOOH catalyst was composed of not only the CoPd alloy NPs with a high concentration of Pd but also isolated Co species, although the latter exhibited little activity for the reaction (Table 1, entry 3). Neither large isolated CoO_x particles nor particles with a high Co composition were observed by microscopic analysis. To account for such differences, more detailed investigations of the CoPd-DDAO/AlOOH were performed by other spectroscopic methods.

XRD patterns of CoPd-capped/AlOOH

To gain more insight into the bimetallic CoPd alloy, the XRD patterns were obtained for the CoPd-capped/AlOOH catalysts and various AlOOH-supported monometallic and bimetallic catalysts (Figure 3A). Diffraction peaks of the AlOOH structure appeared at $2\theta = 14.04$, 28.36, 38.42, 49.06, 55.14, 64.94, and 71.84° for all catalysts. No diffraction signals that correspond to CoO or Co_3O_4 were found in any samples (Figure S6). This indicates that either these species were absent or that the crystalline sizes of the isolated Co species were too small to be detected by XRD. At a 2θ value of around 40°, the bimetallic CoPd NPs catalyst showed a diffraction peak at higher 2θ values in comparison to Pd-DDAO/AlOOH (Figure 3c–g). The area of $2\theta = 36$–44° is shown in Figure 3B to highlight the differences in monometallic and bimetallic catalysts. A similar shift for the (111) lattice spacing of the CoPd (also observed as a striped pattern for the closed packing plane of the face-centered cubic (fcc) structure in TEM) has been reported.[37,53] The shift in the diffraction peak for the bimetallic nanostructure could be explained in terms of d–d bonding and the s–d charge transfer effects as reported for other bimetallic systems such as Ni/Pt, Pd/Au, and Pd/Ag.[54,55]

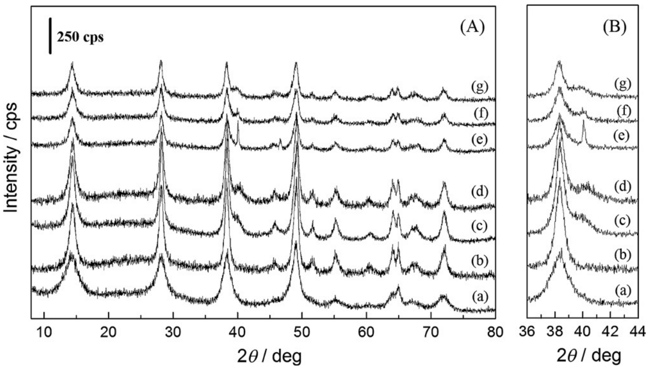

Figure 3. A) XRD patterns in the range of $2\theta = 8$–80° and B) with emphasized detail in the range of $2\theta = 36$–44° of a) AlOOH, b) Co-DDAO/AlOOH, c) Pd-DDAO/AlOOH, d) CoPd-DDAO/AlOOH, e) CoPd-CTAB/AlOOH, f) CoPd-PVP/AlOOH, and g) CoPd/AlOOH.

An intense line that corresponds to CoPd in the XRD pattern of CoPd-CTAB/AlOOH (Figure 3e) implies the presence of large crystals of the bimetallic CoPd particles (crystalline size in the (111) plane is estimated to be 49.4 nm), although these were hardly observed in TEM analysis. CoPd-DDAO/AlOOH has a stable structure under the reaction conditions; similar electron micrographs (Figure 2f and l) and XRD patterns (Figure S7) are obtained even after the fifth catalytic run of the MAn hydrogenation.

XPS of supported CoPd catalysts

XPS measurements were employed to investigate the oxidation states of Co and Pd species and the effect of alloying on each. The Pd 3d states of the various catalysts are shown in Figure 4, in which the Pd $3d_{5/2}$ spectral lines are observed at a binding energy (BE) around 334 eV. A significant negative shift in the BE values for all catalysts was noticed in comparison to pure Pd (BE = 335.1 eV).[56–60] The BEs of the Pd 3d state in these catalysts are attributed to the electron-rich metallic state of Pd as they were much lower than that of palladium oxide (BE = 337.0 eV).[56–60] In the cases of bimetallic CoPd catalysts, negative shifts in BE supposedly indicate an electron transfer phenomenon from Co to Pd in CoPd NP, which is in agreement with the Pauling electronegativities of Pd (2.2) and Co (1.88).

Additionally, from comparison of the capped and noncapped bimetallic CoPd catalysts, the low BE (334.0 eV) of the noncapped bimetallic CoPd catalyst (CoPd/AlOOH) could be distinguished from other capped bimetallic CoPd catalysts, for which the energy of the Pd $3d_{5/2}$ position increased in order from CoPd-DDAO/AlOOH (334.2 eV) to CoPd-PVP/AlOOH (334.4 eV) and CoPd-CTAB/AlOOH (334.5 eV). The higher BEs of the capped CoPd catalysts than noncapped CoPd/AlOOH could be accounted for by the synergistic effect because of the coordination of the capping agent. If the capping agent coordinates to metal NPs, electron donation from the capping

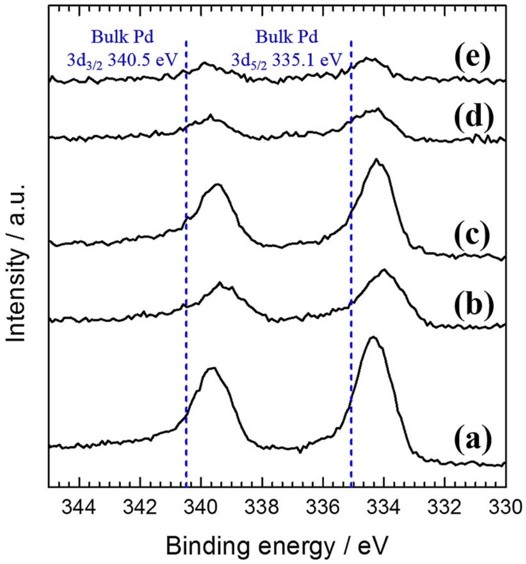

Figure 4. XPS spectra of the Pd 3d states of a) Pd-DDAO/AlOOH, b) CoPd/AlOOH, c) CoPd-DDAO/AlOOH, d) CoPd-PVP/AlOOH, and e) CoPd-CTAB/AlOOH.

agent to the coordinated metal is expected. As it may enhance the negative flow onto Pd atoms in bimetallic CoPd NPs, back donation from d states in Pd towards neighboring Co and/or the capping agent (CTAB, PVP, DDAO) occurs. These synergistic phenomena supposedly determine the back shifts in capped CoPd catalysts to higher energy BE values compared with the noncapped CoPd catalyst. Among the three capped CoPd catalysts, DDAO favored electron-rich Pd in CoPd NPs. However, the Pd $3d_{5/2}$ peak for monometallic Pd-DDAO/AlOOH (29% yield) appeared at BE = 334.3 eV (Figure 4), a little higher than that of bimetallic CoPd-DDAO/AlOOH (BE = 334.2 eV), which possesses higher catalytic activity (>99% yield). Thus, further effects of the coexistence of Co in bimetallic CoPd catalysts need to be discussed (vide infra).

It was expected from the XPS spectra at the Co 2p level that the Co in the catalysts exists as an oxide (CoO and Co_3O_4) instead of metallic Co. Typically, in the case of CoPd-DDAO/AlOOH, the Co $2p_{3/2}$ peak was observed at BE = 780.2–780.9 eV (Figure S8), which is consistent with the BEs of cobalt oxides (bulk CoO BE = 780.6 eV and bulk Co_3O_4 BE = 780.7 eV).[61–63] The absence of a reducing agent such as H_2 during the synthesis of CoPd catalysts is considered to be one of the reasons for the presence of cobalt oxide.

Significant peak broadening for CoPd-CTAB/AlOOH and CoPd-PVP/AlOOH was observed in both the Pd 3d and Co 2p XPS spectra, which could be because of: 1) various oxidation states of Pd and/or Co species and/or 2) changes in electronic density on the Pd and/or Co. Thus, it is suggested that CTAB- and PVP-capped CoPd catalysts possessed various states in Co and Pd, which is different to the DDAO-capped CoPd catalyst.

On this basis, we summarize tentatively that for CoPd-DDAO/AlOOH: 1) the active CoPd alloy NPs were formed more uniformly (i.e., with fewer variations of species) than other capped CoPd materials, 2) the more electron-rich Pd atoms remained on AlOOH, 3) the most stable Co species in the CoPd alloy was produced (rather than noncapped CoPd), which led to the highest activity for the hydrogenation of MAn using FA.

XAS of CoPd catalysts

XAS has been recognized as a powerful technique for the detailed inspection of the electronic states and structures of nanomaterials.[50,64–67] XAS experiments were, therefore, conducted for bimetallic CoPd catalysts to further clarify the nanostructure and electronic interactions induced by the capping agent. X-ray absorption near-edge structure (XANES) analysis of the catalysts at the Pd K-edge and Co K-edge are shown in Figure S9. Pd K-edge and Co K-edge spectra of reference materials (metal foils, oxides, and salts) are shown in Figure S10. The Pd K-edge XANES features (Figure S9 A) were similar to that of Pd foil, which indicates the presence of zero-valent Pd as the dominant state in the catalysts. In accordance with Co 2p XPS, the Co K-edge XANES analysis (Figure S9 B) had a close resemblance to that of cobalt oxides and was significantly different from that of Co foil.

L-edge XANES analysis, which is an electric-dipole allowed transition (p→d), affords more intense and high-resolution observations.[64,68,69] The most prominent feature in the Pd L_3-edge XANES is the white line (WL) at around 3175 eV, observed because of the excitation of electrons from the degenerate 2p states to the 4d band.[64,68,69] The intensity of the WL is proportional to the number of holes in the *n*d valence band of the transition metal species. It is understood that as the hybridization of the d state becomes weaker, the peak at the L_3 threshold is enhanced.[68,69] The Pd L_3-edge XANES analysis of bimetallic catalysts is shown in Figure 5. For all samples, the XANES intensity was higher than that of Pd black (Pd metal), and thus the partial oxidation of NPs by air or by the coordination of the capping agent and/or the strong hybridization phenomenon of Pd states in each sample is expected. CoPd-CTAB/AlOOH

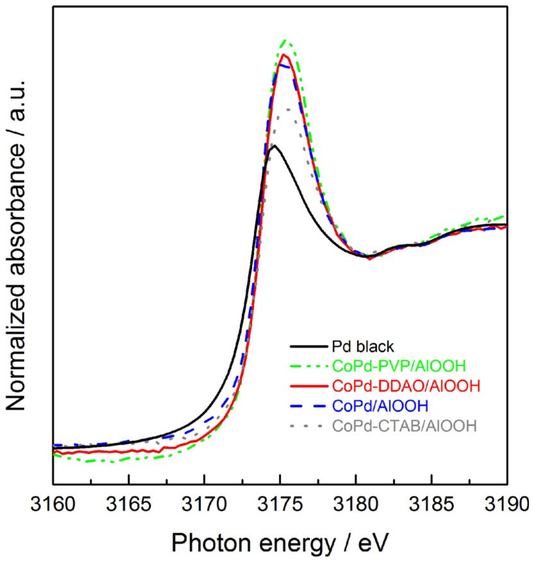

Figure 5. Pd L_3-edge of Pd black and various bimetallic CoPd catalysts.

displayed the lowest WL intensity among the bimetallic catalysts. The WL intensity profiles for CoPd-PVP/AlOOH, CoPd-DDAO/AlOOH, and CoPd/AlOOH were similar and lie above that of CoPd-CTAB/AlOOH. This suggested that the order of electron density in Pd 4d state is CoPd-CTAB/AlOOH > CoPd/AlOOH > CoPd-DDAO/AlOOH > CoPd-PVP/AlOOH. This trend among noncapped and DDAO- or PVP-capped CoPd/AlOOH supports the XPS results for the Pd 3d states.

Thus, the proposed synergistic phenomena between Co, Pd, and the capping agent described in the XPS section are supported here. The CTAB-capped CoPd/AlOOH catalyst demonstrated the highest electron density on Pd 4d. As a result of the large CoPd crystallites observed in the XRD patterns, the surface CTAB on CoPd-CTAB/AlOOH seems to have little influence on the CoPd alloy. Therefore, the electron density profile of CoPd-CTAB/AlOOH in Pd L_3-edge XANES (which includes average information in the sample) differed significantly from that in Pd 3d XPS (which shows surface information selectively).

To understand the detailed structure, we further discuss the extended X-ray absorption fine structure (EXAFS) analysis of these catalysts at both the Pd K- and Co K-edge. The EXAFS at the Pd K-edge and the Fourier transform (FT) of the k^3-weighted Pd K-edge EXAFS data could be hardly distinguished for all catalysts and were similar to that of Pd metal in all cases (Figure S11). This is because of the high concentration of Pd in the CoPd alloy NPs that leads to little information of the Pd–Co interaction in Pd XAS measurements. However, Co K-edge EXAFS analysis would be much informative about the Co–Pd interactions because of the low concentration of Co in the bimetallic CoPd NPs. The Co K-edge EXAFS analysis of the bimetallic CoPd catalysts showed significantly different oscillations from CoO and Co_3O_4 (Figure S12), although they were very similar to that of CoO in the XANES area (Figures S9 and S10). Such marked differences in the EXAFS oscillations from that of the oxide species is strong proof of not only the existence of isolated CoO_x species but also the alloying of Co species with Pd and/or further variety in the bimetallic CoPd catalysts.

The FT of k^3-weighted Co K-edge EXAFS of the three capped bimetallic CoPd catalysts displayed two broadened peaks (Figure S13). Previously,[37] CoPd alloy showed a peak at 2.1 Å with a shoulder at 1.6 Å in the FT of Co K-edge EXAFS data. Although the PVP- and DDAO-capped CoPd catalysts had peaks around 2.35 Å, it is hard to discuss their origin from the FTs at this stage. The FTs of the k^3-weighted EXAFS data of CoPd-DDAO/AlOOH and CoPd-PVP/AlOOH were very different from that of CoPd-CTAB/AlOOH, which had peaks at shorter distances. Additionally, the noncapped bimetallic CoPd catalyst, for which the XRD patterns suggested the presence of CoPd alloy, showed three distinct peaks at 1.44, 1.98, and 2.72 Å. These results implied that each bimetallic CoPd catalyst (capped and noncapped) differed in phase and/or coordination around Co, however, further distinction in the FTs was problematic because of poor information of possible variation and the low concentration of Co species in the catalysts. A detailed study of the structural analysis of the NPs will be published in the near future.

Mechanistic considerations

Based on work by Yoo et al.,[22] we propose that CoPd-DDAO/AlOOH decomposed FA through a dehydrogenation pathway by the adsorbance of FA on oxophilic Co (vide supra) and the enhancement of the rate of FA dissociation. A theoretical approach by Pallassana et al. for the hydrogenation of MAn suggested the adsorption of MAn in a more favorable di-σ conformation on the catalyst surface.[70,71] This is supported by IR spectroscopy performed before and during the reaction to observe the adsorption and thereby the ring-opening of MAn into a diacid on the catalyst surface (Figure S14). As a result of the differences in the electronic charges on the surface of bimetallic CoPd-DDAO/AlOOH and the modification of the Pd–Pd bond distance because of the insertion of Co into the catalyst structure, a better alignment of the surface Pd atoms for improved overlap between the metal d orbitals and the π orbitals of the carbonyl group is expected.[70] Such a geometric effect decreased the adsorption energy, and hence CoPd-DDAO/AlOOH shows an enhanced rate for hydrogenation. These results also suggested that the reaction proceeded over the catalyst surface as proposed in Figure 6.

As the reaction progresses, FA adsorbs on the surface of CoPd-DDAO/AlOOH and CO_2 is released. As a result of the differential charge on CoPd-DDAO/AlOOH (vide supra) the hy-

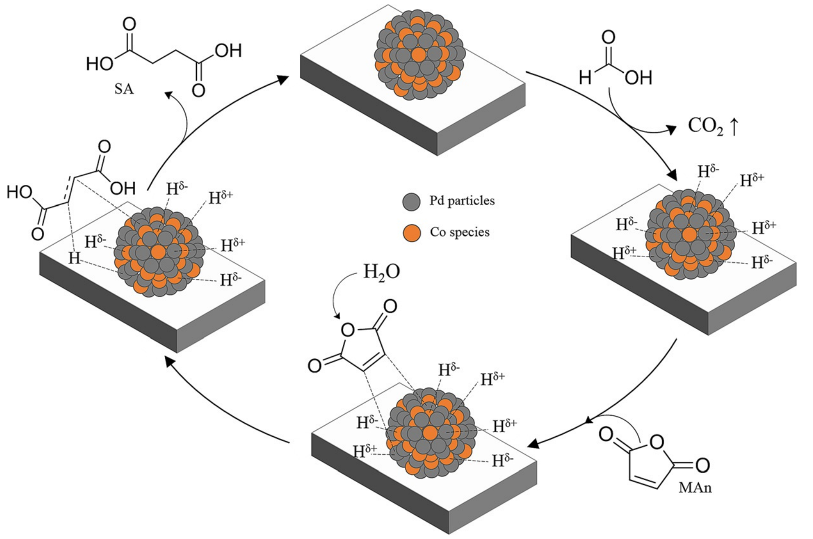

Figure 6. Proposed pathway for the hydrogenation of MAn over CoPd-DDAO/AlOOH using FA as a hydrogen source.

dride dwells on electron-deficient Co species, and Pd, which is electron rich, adsorbs the proton (Figure 6). Simultaneously, MAn attaches to the CoPd surface with a di-σ conformation.[70] The ring opens in water into a diacid form (Figure S14), and the proton from the Pd atom is transferred to the C=C bond. Similarly, another hydrogen atom is transferred to the other carbon atom to produce SA and regenerate the active catalyst. The rate of MAn hydrogenation was found to vary as a function of concentration of both MAn and FA, which indicates competitive adsorption. In accordance with a previous study,[6] we propose the adsorption/dissociation of MAn and/or FA on the catalyst surface as the rate-determining step in this catalysis. These results are in agreement with the activity profiles of CoPd catalysts and also explain the high catalytic activity of CoPd-DDAO/AlOOH. The presence of electron-rich Pd (and oxophilic Co) in CoPd-DDAO/AlOOH accelerated the adsorption and thereby the dissociation of FA under the reaction conditions, and thus an efficient catalysis was observed.

Direct utilization of glucose as a hydrogen source using CoPd-DDAO/AlOOH

Our previous efforts succeeded in the effective production of FA from glucose using the Cu-CTAB/MgO catalyst.[15] The fruitful outcome of hydrogenation using CoPd-DDAO/AlOOH motivated us to combine the two reactions into a one-pot, two-step strategy (Scheme 1). This strategy focused on the synthesis and utilization of FA in the same reaction flask. We elucidated that the filtration of Cu-CTAB/MgO after step 1 and maintaining the temperature at 393 K for hydrogenation could allow the use of glucose as a hydrogen source to yield 8% SA after 3 h (Table S3).

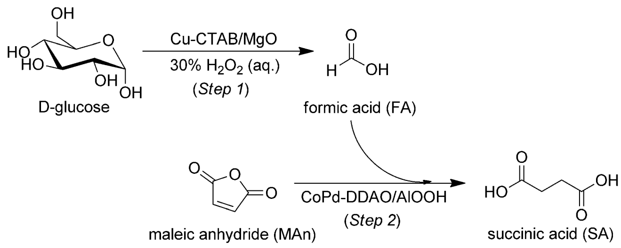

Scheme 1. Hydrogenation of MAn using glucose as a hydrogen source through FA formation.

Conclusions

The preparation of CoPd nanoparticles capped with *N*,*N*-dimethyldodecylamine *N*-oxide (DDAO) supported on AlOOH (CoPd-DDAO/AlOOH) was performed under hydrothermal conditions without a reducing agent. The DDAO-capped bimetallic CoPd catalyst exhibited higher activity than the corresponding monometallic or bimetallic CoPd catalysts with other capping agents (such as poly(*N*-vinyl-2-pyrrolidone) or cetyltrimethylammonium bromide; CTAB) for the hydrogenation of maleic anhydride using formic acid as a sustainable hydrogen source and it could be reused effectively. Electron microscopy observations show that CoPd-DDAO/AlOOH had a mean particle size of 6.4 nm with uniform distribution of Co and Pd within each bimetallic CoPd nanoparticle. XRD, X-ray photoelectron spectroscopy, and X-ray absorption spectroscopy suggested the presence of Co–Pd interactions in the bimetallic CoPd catalyst. Furthermore the alloying of Co with Pd in the presence of DDAO afforded electron-rich Pd and modified the Pd–Pd bond distance. The electron-rich Pd enhanced the adsorption/dissociation of substrates, and the change in interatomic distances facilitated a better alignment of the metal d orbital with the carbonyl π orbitals on the catalyst surface, which enhanced the rate of maleic anhydride hydrogenation into succinic acid. Additionally, CoPd-DDAO/AlOOH in combination with Cu-CTAB/MgO provides a possibility for the direct utilization of abundant biomass-based glucose as a hydrogen source for various hydrogenation reactions. This paper introduces a hydrothermal strategy to create robust supported bimetallic nanoparticles in the presence of a capping agent.

Experimental Section

Chemicals

Cobalt acetate ($Co(OAc)_2{\cdot}4\,H_2O$), palladium acetate ($Pd(OAc)_2$), AlOOH,[72] 5 wt% Pd/Al_2O_3, D-(+)-glucose, CTAB, FA, $Cu(NO_3)_2{\cdot}6\,H_2O$, 30% H_2O_2, and standard solutions (1000 ppm) of palladium and cobalt were purchased from Wako Pure Chemical Industries, Ltd. Acetic acid, SA, MgO, and H_2SO_4 were procured from Kanto Chemical Co., Inc. Tokyo Chemical Industry Co., Ltd. supplied MAn and fumaric acid, whereas DDAO was obtained from Sigma–Aldrich, Co. LLC. Acros Organics provided PVP (K12, average molecular weight 3500).

Catalyst preparation

Surfactant/polymer-capped mono- or bimetallic NPs supported on AlOOH were synthesized by a hydrothermal method as demonstrated previously with some modifications.[15] Typically, $Co(OAc)_2{\cdot}4\,H_2O$ (0.42 mmol) and/or $Pd(OAc)_2$ (0.24 mmol) were dispersed in acetic acid (150 µL) and capping agent (0.5 mmol), followed by the addition of water (3 mL) into the paste. AlOOH (1.0 g) was dispersed in deionized water (25 mL), to which the metal/capping agent solution was added dropwise under stirring. The mixture was stirred vigorously 3 h at RT. The obtained mixture was sealed in a 100 mL Teflon-lined autoclave, heated to 453 K at a heating rate of 6 K min^{-1} in an oven, and maintained at the same temperature for 24 h. The oven was allowed to cool slowly to RT. The obtained solid was washed with deionized water until the pH of the filtrate was neutral, followed by washing with ethanol before drying in vacuo overnight at RT.

Catalytic testing

All experiments to test the catalytic activity were performed in a 50 mL Teflon-lined autoclave unless otherwise stated. The catalytic activity was evaluated for MAn hydrogenation into SA in an aqueous medium. Typically, MAn (0.5 mmol) was dissolved in deionized water (5 mL). Catalyst (25 mg) was added to the solution, followed by the addition of FA (1.9 mmol). The autoclave was sealed and mounted in a preheated oil bath at 353 K. The mixture was allowed to react for various time intervals with continuous magnetic stirring. After the reaction, a part of the resultant solution was diluted 20 times with deionized water, and the catalyst was removed by filtration through a Milex-LG 0.20 μm filter. The obtained filtrate was analyzed by HPLC (WATERS 600) by using an Aminex HPX-87H column (Bio-Rad Laboratories, Inc.) attached to a refractive index detector. Aqueous 10 mM H_2SO_4 (as a mobile phase) was run through the column (maintained at 323 K) at a flow rate of 0.5 mL min^{-1}. The conversion and yield(s) were determined with a calibration curve method.

Recycling tests were performed to check the stability of the synthesized CoPd-DDAO/AlOOH catalyst during the reaction. The catalyst was separated from the reaction mixture by centrifugation. The supernatant liquid was stored, and the analysis of products and the leaching test of catalysts were performed. The residual catalyst was washed by centrifugation with deionized water. Finally, the catalyst was dried in vacuo overnight. Fresh substrates and reagents were added to the catalyst, and the reaction was performed again.

Characterization

The crystal structure was analyzed by powder X-ray diffraction (PXRD) by using a SmartLab diffractometer (Rigaku Co.) using CuK$_\alpha$ radiation ($\lambda = 0.154$ nm) at 40 kV and 30 mA in the range of $2\theta = 8$–80°. The diffraction patterns were analyzed using the database of the Joint Committee of Powder Diffraction Standards (JCPDS). For ICP-AES, an ICPS-7000 ver. 2 (Shimadzu Co.) was employed to quantify the real amounts of Co and Pd on AlOOH and to evaluate metal leaching, if any, during the reaction. Contents of metal (Co and/or Pd) in the catalyst and/or the reaction medium were estimated by a calibration curve method using the standard solutions. An H-7650 TEM (Hitachi, Ltd.) operating at 100 kV was utilized to acquire the morphology of catalyst. HAADF-STEM images and elemental mapping analyses were recorded by using a JEM-ARM200F (JEOL USA, Inc.) that operated at 200 kV. The samples for TEM measurements were dispersed in water, and the supernatant liquid was dropped onto a copper/carbon grid before drying in vacuo overnight. The electronic state of Co/Pd on AlOOH was analyzed by XPS. The experiments were conducted by using an AXIS-ULTRA DLD spectrometer system (Shimadzu Co. and Kratos Analytical Ltd.) using an Al target at 15 kV and 10 mA in an energy range of 0–1200 eV. The BEs were calibrated with the C 1s level (284.5 eV) as an internal standard reference. XAS was performed by using BL-9C (Co K-edge) and BL-9 A (Pd L_3-edge) at KEK-PF under the approval of the Photon Factory Program Advisory Committee (Proposal No. 2013G586) and BL01B1 (Pd K-edge) at SPring-8 under the approval of the Japan Synchrotron Radiation Research Institute (JASRI; Proposal Nos. 2013B1478 and 2014B1472). FTs of k^3-weighted EXAFS data were performed in the range of 3–12 Å^{-1} for Co K and 3–13 Å^{-1} for Pd K-edge XAS. All samples were ground and pressed to pellets with a diameter of 10 mm. The obtained XAS spectra were analyzed by using Rigaku REX2000 software (ver. 2.5.92). The IR measurements of samples were performed by using a PerkinElmer Spectrum 100 FTIR spectrometer.

Acknowledgements

We greatly appreciate Dr. Koichi Higashimine (JAIST, Center for Nano Materials and Technology) and Dr. Hitoshi Abe (KEK-PF) for their support in HADDF-STEM-EDS and XAS (KEK-PF) studies, respectively. H.C. extends his thanks to the Japan Society for the Promotion of Science (JSPS) for a fellowship and KAKENHI (No. 26-12396; Grant-in-Aid for JSPS Fellows). This work is partially supported by KAKENHI (No. 25820392; Grant-in-Aid for Young Scientists (B)) and the Mitani Foundation for Research and Development.

Keywords: formic acid · hydrogenation · capping agent · palladium · supported catalysts

[1] V. Mazumder, S. Sun, *J. Am. Chem. Soc.* **2009**, *131*, 4588–4589.
[2] V. Mazumder, Y. Lee, S. Sun, *Adv. Funct. Mater.* **2010**, *20*, 1224–1231.
[3] A. Majewski, D. J. Morris, K. Kendall, M. Wills, *ChemSusChem* **2010**, *3*, 431–434.
[4] A. Boddien, D. Mellmann, F. Gartner, R. Jackstell, H. Junge, P. J. Dyson, G. Laurenczy, R. Ludwig, M. Beller, *Science* **2011**, *333*, 1733–1736.
[5] K. Tedsree, T. Li, S. Jones, C. W. A. Chan, K. M. K. Yu, P. A. J. Bagot, E. A. Marquis, G. D. W. Smith, S. C. E. Tsang, *Nat. Nanotechnol.* **2011**, *6*, 302–307.
[6] V. Mazumder, M. Chi, M. N. Mankin, Y. Liu, O. Metin, D. Sun, K. L. More, S. Sun, *Nano Lett.* **2012**, *12*, 1102–1106.
[7] F. Joó, *ChemSusChem* **2008**, *1*, 805–808.
[8] T. C. Johnson, D. J. Morris, M. Wills, *Chem. Soc. Rev.* **2010**, *39*, 81–88.
[9] M. Grasemann, G. Laurenczy, *Energy Environ. Sci.* **2012**, *5*, 8171–8181.
[10] W. Gan, P. J. Dyson, G. Laurenczy, *ChemCatChem* **2013**, *5*, 3124–3130.
[11] S. Enthaler, A. Bruck, A. Kammer, H. Junge, E. Irran, S. Gulak, *ChemCatChem* **2015**, *7*, 65–69.
[12] J. J. Bozell, *Science* **2010**, *329*, 522–523.
[13] R. Xing, W. Qi, G. W. Huber, *Energy Environ. Sci.* **2011**, *4*, 2193–2205.
[14] Z. Tang, W. Deng, Y. Wang, E. Zhu, X. Wan, Q. Zhang, Y. Wang, *ChemSusChem* **2014**, *7*, 1557–1567.
[15] H. Choudhary, S. Nishmura, K. Ebitani, *Appl. Catal. B* **2015**, *162*, 1–10.
[16] J. H. A. Martens, R. Prins, D. C. Konningsberger, *J. Phys. Chem.* **1989**, *93*, 3179–3185.
[17] R. W. Wunder, J. Phillips, *J. Phys. Chem.* **1996**, *100*, 14430–14436.
[18] S. Nishimura, Y. Yakita, M. Katayama, K. Higashimine, K. Ebitani, *Catal. Sci. Technol.* **2013**, *3*, 351–359.
[19] D. Tongsakul, S. Nishimura, K. Ebitani, *ACS Catal.* **2013**, *3*, 2199–2207.
[20] D. Tongsakul, S. Nishimura, K. Ebitani, *J. Phys. Chem. C* **2014**, *118*, 11723–11730.
[21] J. Wang, G. Yin, Y. Chen, R. Li, X. Sun, *Int. J. Hydrogen Energy* **2009**, *34*, 8270–8275.
[22] J. S. Yoo, F. Ablid-Pedersen, J. K. Nørskov, F. Studt, *ACS Catal.* **2014**, *4*, 1226–1233.
[23] J. L. Fernández, D. A. Walsh, A. J. Bard, *J. Am. Chem. Soc.* **2005**, *127*, 357–365.
[24] V. Raghuveer, A. Manthiram, A. J. Bard, *J. Phys. Chem. B* **2005**, *109*, 22909–22912.
[25] M. H. Shao, K. Sasaki, R. R. Adzic, *J. Am. Chem. Soc.* **2006**, *128*, 3526–3527.
[26] N. Toshima, T. Yonezawa, *New J. Chem.* **1998**, *22*, 1179–1201.
[27] B. L. Cushing, V. L. Kolesnichenko, C. J. O'Connor, *Chem. Rev.* **2004**, *104*, 3893–3946.
[28] R. Ferrando, J. Jellinek, R. L. Johnston, *Chem. Rev.* **2008**, *108*, 845–910.
[29] T. K. Sau, A. L. Rogach, *Adv. Mater.* **2010**, *22*, 1781–1804.
[30] M. Sankar, N. Dimitratos, P. J. Miedziak, P. P. Wells, C. J. Kiely, G. J. Hutchings, *Chem. Soc. Rev.* **2012**, *41*, 8099–8139.
[31] B. H. Kim, M. J. Hackett, J. Park, T. Hyeon, *Chem. Mater.* **2014**, *26*, 59–71.
[32] A. K. Singh, Q. Xu, *ChemCatChem* **2013**, *5*, 652–676.
[33] I. Notar Francesco, F. Fontaine-Vive, S. Antoniotti, *ChemCatChem* **2014**, *6*, 2784–2791.
[34] D. Wu, M. Cao, M. Shen, R. Cao, *ChemCatChem* **2014**, *6*, 1731–1736.
[35] M. Cao, J. Lin, H. Yang, R. Cao, *Chem. Commun.* **2010**, *46*, 5088–5090.
[36] P. Lu, T. Teranishi, K. Asakura, M. Miyake, N. Toshima, *J. Phys. Chem. B* **1999**, *103*, 9673–9682.
[37] S. Takenaka, T. Tsukamoto, H. Matsune, M. Kishida, *Catal. Sci. Technol.* **2013**, *3*, 2723–2731.

[38] D. Wu, M. Cao, R. Cao, *Chem. Commun.* **2014**, *50*, 12970 – 12972.
[39] G. Demazeau, *J. Mater. Chem.* **1999**, *9*, 15 – 18.
[40] J. Li, Z. Chen, R. J. Wang, D. M. Proserpio, *Coord. Chem. Rev.* **1999**, *190–192*, 707 – 735.
[41] K. Byrappa, T. Adschiri, *Prog. Cryst. Growth Charact. Mater.* **2007**, *53*, 117 – 166.
[42] C. Delhomme, D. Weuster-Botz, F. E. Kühn, *Green Chem.* **2009**, *11*, 13 – 26, and references cited therein.
[43] J. Tuteja, H. Choudhary, S. Nishimura, K. Ebitani, *ChemSusChem* **2014**, *7*, 96 – 100.
[44] P. A. Son, S. Nishimura, K. Ebitani, *RSC Adv.* **2014**, *4*, 10525 – 10530.
[45] J. Tuteja, S. Nishimura, K. Ebitani, *RSC Adv.* **2014**, *4*, 38241 – 38249.
[46] N. Toshima, M. Harada, T. Yonezawa, K. Kushihashi, K. Asakura, *J. Phys. Chem.* **1991**, *95*, 7448 – 7453.
[47] M. Harada, K. Asakura, Y. Ueki, N. Toshima, *J. Phys. Chem.* **1993**, *97*, 10742 – 10749.
[48] Y. Wang, N. Toshima, *J. Phys. Chem. B* **1997**, *101*, 5301 – 5306.
[49] H. Zhang, T. Watanbe, M. Okumura, M. Haruta, N. Toshima, *Nat. Mater.* **2012**, *11*, 49 – 52.
[50] S. Nishimura, D. Mott, A. Takagaki, S. Maenosono, K. Ebitani, *Phys. Chem. Chem. Phys.* **2011**, *13*, 9335 – 9343.
[51] The turnover number for the hydrogenation of MAn (0.5 mmol) with the CoPd-DDAO/AlOOH is 84 based on the total amount of Pd in the catalyst.
[52] The ICP-AES analysis of the reaction mixture after a catalytic run also underlined the stability of AlOOH (or nonleaching of Al) under the reaction conditions irrespective of the presence or absence of capping agents during catalyst preparation.
[53] D. Sun, V. Mazumder, Ö. Metin, S. Sun, *ACS Nano* **2011**, *5*, 6458 – 6464.
[54] E. G. Allison, G. C. Bond, *Catal. Rev.* **1972**, *7*, 233 – 289.
[55] J. M. Dominguez, A. Vazquez, A. J. Renouprez, M. J. Jose Yacaman, *J. Catal.* **1982**, *75*, 101 – 111.
[56] B. Schleich, D. Schmeisser, W. Gopel, *Surf. Sci.* **1987**, *191*, 367 – 384.
[57] J. M. Tura, P. Regull, L. Victori, M. Dolors de Castellar, *Surf. Interface Anal.* **1988**, *11*, 447 – 449.
[58] I. Z. Shyu, K. Otto, W. L. H. Watkins, G. W. Graham, R. K. Belitz, H. S. Gandhi, *J. Catal.* **1988**, *114*, 23 – 33.
[59] T. J. Sarapatka, *J. Phys. Chem.* **1993**, *97*, 11274 – 11277.
[60] C. J. Jenks, S. L. Chang, J. W. Anderegg, P. A. Thiel, D. W. Lynch, *Phys. Rev. B* **1996**, *54*, 6301 – 6306.
[61] T. J. Chuang, C. R. Brundle, D. W. Rice, *Surf. Sci.* **1976**, *59*, 413 – 429.
[62] M. Oku, K. Hirokawa, *J. Electron Spectrosc. Relat. Phenom.* **1976**, *8*, 475 – 481.
[63] B. J. Tan, K. J. Klabunde, P. M. A. Sherwood, *J. Am. Chem. Soc.* **1991**, *113*, 855 – 861.
[64] *X-ray Absorption: Techniques of EXAFS, SEXAFS and XANES* (Eds.: D. C. Koningsberger, R. Prins), Wiley, New York, **1988**.
[65] M. Harada, K. Asakura, N. Toshima, *J. Phys. Chem.* **1994**, *98*, 2653 – 2662.
[66] U. Kolb, S. A. Quaiser, M. Winter, M. T. Reetz, *Chem. Mater.* **1996**, *8*, 1889 – 1894.
[67] S. Nishimura, A. T. N. Dao, D. Mott, S. Maenosono, K. Ebitani, *J. Phys. Chem. C* **2012**, *116*, 4511 – 4516.
[68] T. K. Sham, *Phys. Rev. B* **1985**, *31*, 1888 – 1902.
[69] T. K. Sham, *Phys. Rev. B* **1985**, *31*, 1903 – 1908.
[70] V. Pallassana, M. Neurock, G. W. Coulston, *J. Phys. Chem. B* **1999**, *103*, 8973 – 8983.
[71] V. Pallassana, M. Neurock, *J. Phys. Chem. B* **2000**, *104*, 9449 – 9459.
[72] The BET surface area and pore volume of the boehmite employed in this study are 465 $m^2 g^{-1}$ and 0.79 $mL g^{-1}$, respectively.

Received: February 17, 2015